Supporting Information

Zn^{2+}-Coordinated Hierarchical Dynamic Crosslinking in Phenolized Lignin-Based Polyurethane Elastomers: Mechanical Self-Reinforcement and Dynamic Adaptability Enhancement

Yaling Xu[a], Shusheng Chen[b,c,d*], Weifeng Liu[a,c*], Xueqing Qiu[c,d]

[a] School of Chemistry and Chemical Engineering, State Key Laboratory of Advanced Papermaking and Paper-based Materials, Guangdong Provincial Key Lab of Green Chemical Product Technology, South China University of Technology, Guangzhou 510640, P. R. China.

[b] School of Advanced Manufacturing, Guangdong University of Technology, Jieyang 515200, P. R. China.

[c] Guangdong Provincial Laboratory of Chemistry and Fine Chemical Engineering Jieyang Center, Jieyang 515200, P. R. China.

[d] Guangdong Provincial Key Laboratory of Plant Resources Biorefinery, School of Chemical Engineering and Light Industry, Guangdong University of Technology, Guangzhou 510006, P.R. China.

[*]**Corresponding Authors:**

[*] E-mail: shusheng.chen@gdut.edu.cn

[*] E-mail: weifengliu@scut.edu.cn

Experimental section

1 Materials

Industrial alkali lignin (AKL, 99%) was purchased from Shanghai Changfa New Material Co., Ltd. Poly(tetramethylene ether) glycol (PTMG1000, AR), hexamethylene diisocyanate (HDI, AR), dibutyltin dilaurate (DBTDL, AR), absolute ethanol, and N,N-dimethylformamide (DMF, 99%) were obtained from Aladdin Reagent (Shanghai) Co., Ltd. Tetrahydrofuran (THF), dimethyl sulfoxide (DMSO, 99%), and catechol (99.5%) were supplied by Macklin Biochemical Technology Co., Ltd. (Shanghai). Zinc chloride ($ZnCl_2$, 0.5 mol/L in THF) was procured from Energy Chemical Co., Ltd. Concentrated sulfuric acid (96%) was acquired from Shanghai Sushi Chemical Co., Ltd.

2 Preparation of Ethanol-extracted lignin (AOH)

Industrial alkali lignin (AKL) was purified via ethanol-based liquid-solid extraction to obtain lignin with higher hydroxyl content (AOH). Specifically, 200 g of AKL was dissolved in 1 L of anhydrous ethanol, stirred at room temperature for 2 h, and filtered to collect the filtrate, which was then concentrated by rotary evaporation. The resulting product was dried in a vacuum oven at 55 °C for 48 h to yield AOH.

3 Synthesis of Phenolized Lignin (CAL)

Phenolized lignin (CAL) was synthesized by blending catechol with dried industrial alkali lignin (AKL) at a mass ratio of 3:1 at 140 °C for 1 h under condensate reflux. After the lignin was fully dissolved in catechol, concentrated sulfuric acid (approximately 11 wt% relative to lignin) was added dropwise in a controlled manner

at 110 °C, and the reaction proceeded for 2 h. Upon completion, dimethyl sulfoxide (DMSO) was promptly added to dissolve the product, and the system was cooled to room temperature. The phenolized lignin was subsequently precipitated by pouring the solution into an excess of dilute sulfuric acid solution (PH = 1.5). The resulting solid was collected by filtration, thoroughly washed with deionized water, and dried in a vacuum oven at 55 °C for approximately 24 h to yield the final product, CAL. The synthesis route is illustrated in Figure S1.[1]

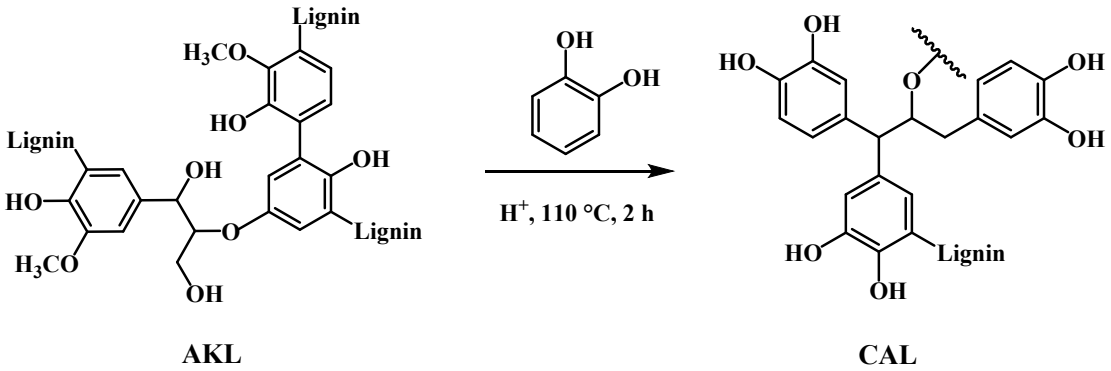

Figure S1. Schematic diagram of CAL synthesis.[1]

4 Synthesis of Zn-LPUes

A predetermined amount of PTMEG1000 (according to Table S1) was weighed into a three-necked flask, placed in an oil bath, and heated to 120 °C with stirring. Dehydration was performed under vacuum for 1 h. The temperature was then lowered to 70 °C, followed by the sequential addition of 10 mL of THF, 0.05 g of DBTDL, and a specified mass of HDI. The reaction proceeded under a nitrogen atmosphere for 2 h to form the polyurethane prepolymer.

Subsequently, a measured amount of lignin (AOH or CAL) was dissolved in 10 mL of THF and added to the prepolymer system, with the reaction continuing for

another 2 h. A specified volume of $ZnCl_2$ solution in THF (according to Table S1) was then added via micropipette. The reaction was stopped once noticeable climbing of the product along the stirrer shaft was observed. The resulting product was collected and dried in a vacuum oven at 55 °C for 12 h to remove the solvent. Finally, the dried product was cut into small pieces and hot-pressed at 165 °C and 10 MPa for 10 min to obtain films designated as XAOH-R-Y or XCAL-R-Y. Here, X represents the mass percentage of AOH or CAL relative to the total mass of the hydroxyl-containing components, R denotes the isocyanate index, and Y indicates the mass percentage of $ZnCl_2$ relative to the total system mass.

Table S1. Synthesis formula of Zn-LPUes.

Sample	AOH (g)	CAL (g)	PTMG1000 (g)	HDI (g)	R value	volume of $ZnCl_2$ solution in THF (μL)
10AOH-1.2-1	0.80	—	7.20	1.81	1.2	1439
10CAL-1.2-1	—	0.80	7.20	1.81	1.2	1439
5CAL-1.2-1	—	0.40	7.60	1.71	1.2	1425
20CAL-1.2-1	—	1.60	6.40	2.00	1.2	1468
10CAL-1.0-1	—	0.80	7.20	1.51	1.0	1395
10CAL-1.1-1	—	0.80	7.20	1.66	1.1	1417
10CAL-1.3-1	—	0.80	7.20	1.96	1.3	1461
10CAL-1.2-0	—	0.80	7.20	1.81	1.2	0
10CAL-1.2-0.5	—	0.80	7.20	1.81	1.2	719
10CAL-1.2-1.5	—	0.80	7.20	1.81	1.2	2158

5 Characterization

All samples were dried in a vacuum oven at 50 °C for 12 h prior to testing.

The relative molecular mass of lignin was determined using an organic-phase gel permeation chromatography (1260 Infnity II, Agilent, Germany). Lignin was dissolved in tetrahydrofuran (THF) at a concentration of approximately 2 mg/mL. Chromatographic grade THF was used as the mobile phase with a flow rate of 1.0 mL/min.

^{31}P NMR (Phosphorus-31 Nuclear Magnetic Resonance Spectroscopy) of phenolized lignin (CAL), ethanol-extracted lignin (AOH), and industrial alkali lignin (AKL) was characterized using an AVANCE III HD 600 MHz spectrometer (Bruker, Germany). A mixed solvent was prepared by combining deuterated pyridine and deuterated chloroform in a volume ratio of 1.6:1. The internal standard solution was prepared by dissolving 0.018 g of internal standard (N-hydroxy-5-norbornene-2,3-dicarboximide) and 0.005 g of relaxation agent (chromium(III) 2,4-pentanedionate) in 1 mL of the mixed solvent. For NMR sample preparation, 30 mg of lignin was dissolved in 0.5 mL of the mixed solvent, followed by the addition of 0.1 mL of the internal standard solution. After magnetic stirring for 12 h, 0.15 mL of the phosphitylation reagent (2-chloro-4,4,5,5-tetramethyl-1,3,2-dioxaphospholane) was added. The measurement was performed at room temperature with a 90° pulse angle, a 25 s pulse delay, 250 scans, and a spectral width of 61.9 ppm. The hydroxyl content of lignin was calculated using the following formula:

$$C_{OH} = \frac{m_1}{179.17} \times 0.99 \times 1000 \times \frac{m_{IS}}{m_1 + m_2 + m_3} \times \frac{A_{OH}}{A_{IS} + m_L} \#(1)$$

where C_{OH} (mmol/g) is the hydroxyl content of lignin, m_{IS} (g) is the mass of the 0.1 mL internal standard solution, m_1 (g) is the mass of the internal standard substance,

m_2 (g) is the mass of the relaxation agent, m_3 (g) is the mass of 1 mL of the solvent, A_{OH} is the peak area of the hydroxyl group, A_{IS} is the peak area of the internal standard, and m_L (g) is the mass of the lignin sample.

Fourier transform infrared spectroscopy (FTIR) of Zn-LPUes was characterized using a total reflection Fourier transform infrared spectrometer (Nicolet iS50, Thermo Scientific, America). Measurements were performed in attenuated total reflectance (ATR) mode with a wavenumber range of 4000 ~ 400 cm^{-1}, 64 scans, and a resolution of 4 cm^{-1}.

The cross-sectional morphology of Zn-LPUes was investigated using a field-emission scanning electron microscope (SU8220, Hitachi, Japan). Samples were immersed in liquid nitrogen for 1-2 minutes, subsequently fractured, and then dried in a vacuum oven at 55 °C for 12 hours. Prior to imaging, the sample surfaces were sputter-coated with a thin gold layer.

The microphase structure of Zn-LPUes was investigated using a field-emission transmission electron microscope (JEM 1400 PLUS, Hitachi, Japan). The samples were cryo-ultramicrotomed into 80 nm thick sections and mounted on copper grids for observation.

The surface elemental composition of the samples was analyzed using X-ray photoelectron spectroscopy (XPS) (Thermo Scientific K-Alpha, America). An appropriately sized sample was mounted on a sample holder and introduced into the instrument's load-lock chamber. Once the chamber pressure reached below 5×10^{-7}

mbar, the sample was transferred into the analysis chamber. Measurements were performed with a 400 μm X-ray spot size, an accelerating voltage of 12 kV, and a filament current of 6 mA. Survey scans were acquired with a pass energy of 150 eV and a step size of 1 eV, while high-resolution regional scans were performed with a pass energy of 50 eV and a step size of 0.1 eV.

The mechanical properties and tensile hysteresis behavior of Zn-LPUes were evaluated using an electronic universal testing machine (CMT, Meters Industrial Systems Co., Ltd., China). Samples obtained by hot-pressing were cut into standard dumbbell-shaped specimens (50×4×0.5 mm). Mechanical property testing was conducted according to the GB/T 528-2009/ISO 37:2005 standard at room temperature. Five replicate tests were performed for each sample, and the average values were reported. The tensile speed was set at 100 mm/min. Toughness was determined as the integral area under the stress-strain curve, calculated using Equation (4), while the elastic recovery ratio was defined as the percentage of recovered deformation, calculated using Equation (5). For the fixed-strain tensile hysteresis tests, each specimen was first stretched to a fixed strain of 1000% at a rate of 100 mm/min and subsequently unloaded to its initial state at the same rate. This cycle was repeated eight times. The hysteresis loss (W_n, in MJ/m^3) for each cycle was obtained by integrating the area of the corresponding hysteresis loop. For the variable-strain tensile hysteresis tests, specimens were subjected to cyclic loading at different strain levels: 100%, 200%, 300%, 400%, 600%, 700%, 800%, 900%, and 1000%, using a constant tensile rate of 100 mm/min.

$$W = \int_{\varepsilon = 0}^{\varepsilon = \varepsilon_{max}} \sigma d\varepsilon \#(2)$$

Where W (MJ/m^3) is the toughness, ε (%) is the tensile strain, and σ (MPa) is the tensile stress.

$$E_R = \frac{L_{max} - L_R}{L_{max} - L_0} \#(3)$$

Where E_R is the elastic recovery ratio, L_{max} (mm) is the maximum length of the specimen at the point of fracture, L_R (mm) is the length of the specimen after recovery following fracture, and L_0 (mm) is the initial length of the specimen.

The segmental orientation of Zn-LPUes was examined using a two-dimensional wide-angle X-ray diffraction (2D-WAXD) system (Rigaku, Japan). Measurements were performed with an X-ray wavelength of 1.5405 Å, an exposure time of 30 s, a Hypix-6000 photon-counting detector, and a sample-to-detector distance of 70 mm. The Herman orientation factor was calculated according to Equations (4) and (5).

$$f = \frac{3 < cos^2\phi > - 1}{2} \#(4)$$

$$< cos^2\phi > = \frac{\int_0^{\pi} I(\phi) cos^2\phi sin\phi d\phi}{\int_0^{\pi} I(\phi) sin\phi d\phi} \#(5)$$

Where $\langle \cos^2\varphi \rangle$ represents the intensity-weighted average of the square of the cosine of the azimuthal angle φ for the oriented crystal plane.

The stress relaxation behavior, viscoelastic properties, and crosslinking density of

Zn-LPUes were measured using a dynamic mechanical analyzer (DMA850, TA Instruments, America). Frequency scans were carried out at 30 ~ 90 °C, controlling strain at 0.1% (within the linear viscoelastic region) and varying the frequency from 1 Hz to 70 Hz. For stress relaxation tests, the samples were heated to the target temperature (ranging from 120 to 160 °C) and held for 3 min, then rapidly stretched to 50% strain. The stress evolution was recorded over a period of 1 h. Viscoelastic behavior was characterized in film tension mode with a temperature sweep from -70 to 100 °C at a heating rate of 3 °C/min. The loss factor, crosslinking density, and relaxation activation energy were calculated according to Equations (6), (7), and (8), respectively.

$$\tan\delta = \frac{E''}{E'} \#(6)$$

Where *tanδ* is the loss factor, E'' (MPa) is the loss modulus, and E' (MPa) is the storage modulus.

$$\upsilon_e = \frac{E_r}{3RT_r} \#(7)$$

Where υ_e (mol/m^3) is the crosslinking density, T_r (K) and E_r (Pa) represent the Kelvin temperature and storage modulus at the temperature of $T_{g\text{-}DMA}$ + 40 °C, respectively, and R (8.314 J·K^{-1}·mol^{-1}) is the ideal gas constant.

$$\ln\tau = \ln\tau_0 + \frac{E_{af}}{RT} \#(8)$$

Where τ (s) is the stress relaxation time, T (K) is the Kelvin temperature, E_{af}

(kJ/mol) is the activation energy for flow, R (8.314 $J \cdot K^{-1} \cdot mol^{-1}$) is the ideal gas constant, and $ln\tau_0$ is a constant.

The transverse relaxation (T_2) experiments were performed using low-field nuclear magnetic resonance (LF-NMR) analyzer (MicroMR12-025 V, Niumag, China) to characterize the relaxation behavior of Zn-LPUes. Signal intensity decay curves as a function of relaxation time were recorded for subsequent analysis.

The thermal stability of Zn-LPUes was evaluated using a thermogravimetric analyzer (TG209F1, Netzsch, Germany). Prior to testing, the samples were vacuum-dried at 50 °C for approximately 12 hours. About 8 mg of the sample was weighed into an alumina crucible. The temperature was then raised from room temperature to 600 °C at a heating rate of 10 °C/min under a continuous nitrogen atmosphere.

The thermal oxygen aging resistance performance of Zn-LPUes was tested using a thermal oxygen aging oven (NR8851, China). The mechanical properties of Zn-LPUes were measured after aging at 100 °C for three days, and the mechanical properties of Zn-LPUes before and after aging were compared.

The photothermal performance and light-controlled self-healing capability of Zn-LPUes were evaluated using an 808 nm near-infrared (NIR) laser (Lasever, China) and a T560 infrared thermal camera (FLIR). For photothermal testing, the samples were irradiated with an NIR laser at specified power densities. The laser head was positioned 10 cm from the sample surface, and the thermal camera was placed 20 cm away. Surface temperature changes were recorded in real time using the thermal camera. For light-

controlled self-healing assessment, the samples were partially cut (approximately 50% through the thickness), and the fractured surfaces were irradiated with the NIR laser to induce healing. The mechanical properties of the samples were compared before and after the light-triggered healing process to evaluate the healing efficiency.

Supporting Figures and Tables

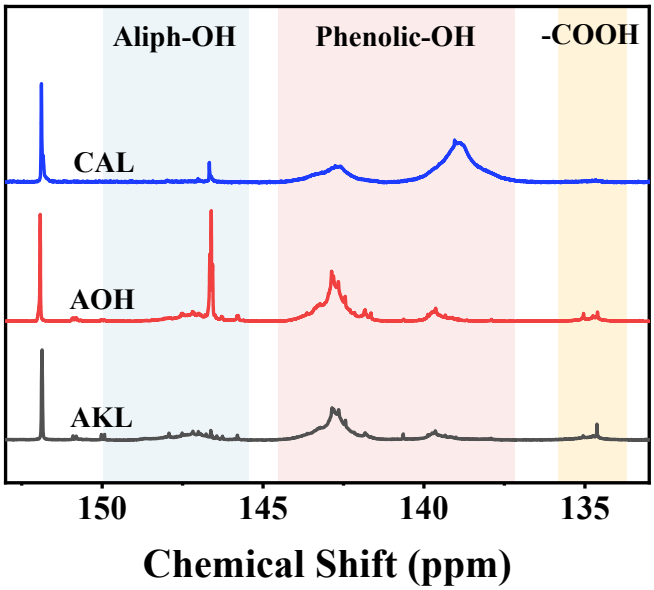

Figure S2. ^{31}P NMR spectra of CAL, AOH, and AKL.

Table S2. The contents of various hydroxyl groups in CAL, AOH and AKL.

Sample	Aliphatic OH (mmol/g)	Phenolic OH (mmol/g)	Total OH (mmol/g)	Mw (g/mol)	Mn (g/mol)	PDI
CAL	0.08	4.34	4.42	835	524	1.59
AOH	1.36	3.13	4.49	858	617	1.31
AKL	0.53	2.28	2.81	2243	1102	2.15

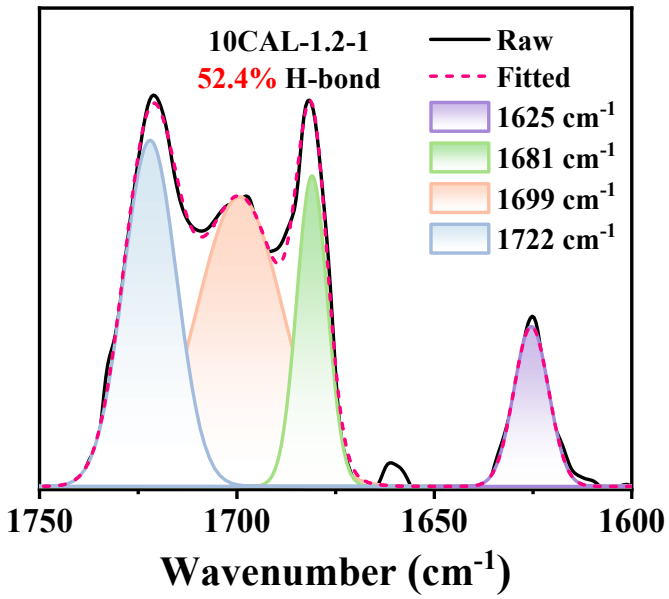

Figure S3. FTIR spectrum of the C=O stretching vibration bands for 10CAL-1.2-1.

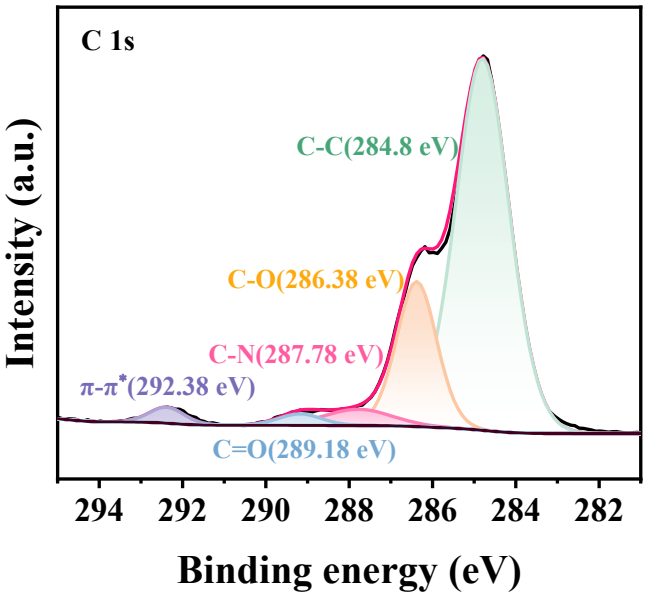

Figure S4. C 1s XPS spectrum of 10CAL-1.2-0.5.

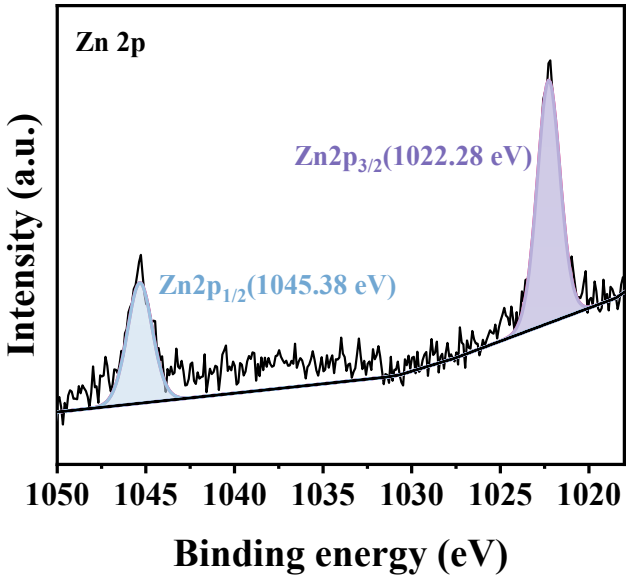

Figure S5. Zn 2p XPS spectrum of 10CAL-1.2-0.5.

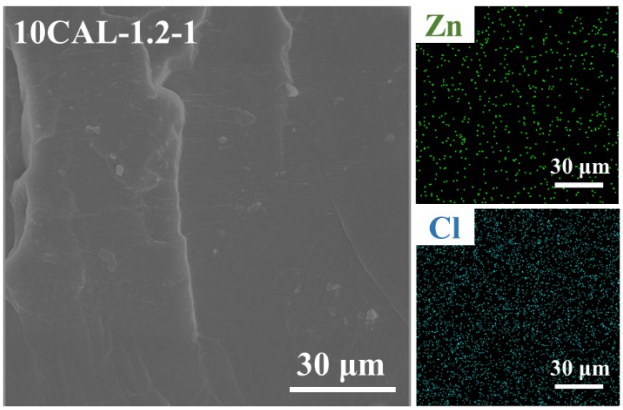

Figure S6. SEM image and EDS mapping image of 10CAL-1.2-1.

Table S3. Mechanical properties of Zn-LPUes.

Sample	Tensile strength (MPa)	Elongation at break (%)	Toughness (MJ/m^3)	Elastic recovery (%)
10AOH-1.2-1	14.2 (±2.1)	1135 (±80)	107.2	94.4
10CAL-1.2-1	34.6 (±4.8)	1585 (±106)	185.1	93.9
5CAL-1.2-1	28.2 (±1.2)	1722 (±124)	232.7	93.8
20CAL-1.2-1	30.9 (±0.4)	1221 (±123)	181.7	93.3
10CAL-1.0-1	11.6 (±1.4)	1793 (±156)	114.8	93.5
10CAL-1.1-1	21.7 (±4.8)	1696 (±92)	171.9	90.0
10CAL-1.3-1	24.5 (±3.5)	1391 (±85)	145.2	91.5
10CAL-1.2-0	37.9 (±3.6)	1408 (±76)	198.9	96.2
10CAL-1.2-0.5	42.8 (±1.7)	1569 (±25)	270.5	94.0

10CAL-1.2-1.5	14.7 (±1.8)	1492 (±82)	118.0	91.0

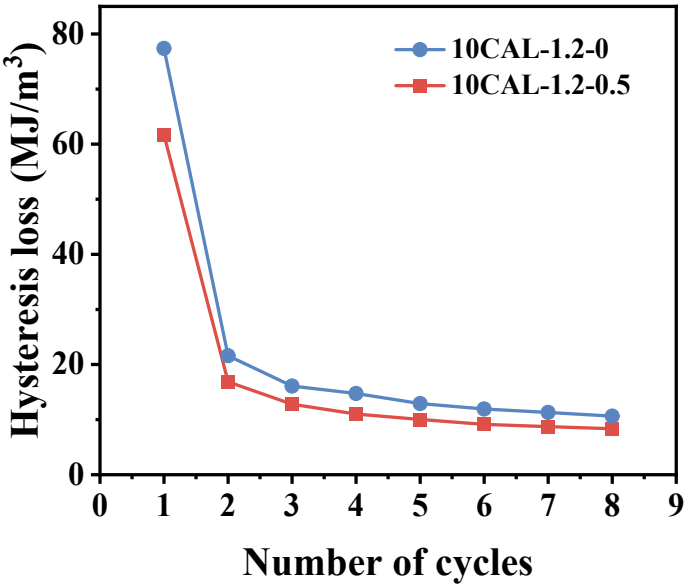

Figure S7. Comparison curve of hysteresis loop areas of Zn-LPUes under different cycle numbers.

Table S4. Mechanical properties of Zn-LPUes after 8 cycles of tensile training with a strain of 1000%.

Sample	Tensile strength (MPa)	Elongation at break (%)	Toughness (MJ/m^3)	Enhancement rate (%)
10CAL-1.2-0	52.0 (±1.3)	1103 (±63)	223.8	37.2
10CAL-1.2-0.5	64.5 (±2.8)	1230 (±107)	329.1	50.7

Table S5. Mechanical properties of 10CAL-1.2-0.5 after different cycles of tensile training with a strain of 1000%.

Number of cycles	Tensile strength (MPa)	Elongation at break (%)	Toughness (MJ/m^3)	Enhancement rate (%)
Original	42.8 (±1.7)	1569 (±25)	270.5	—
1	42.6 (±2.3)	1260 (±89)	229.3	0
4	58.6 (±0.9)	1247 (±76)	288.6	36.9
8	64.5 (±2.8)	1230 (±107)	329.1	50.7
12	50.8 (±1.6)	1176 (±93)	240.9	18.7

Table S6. Mechanical properties of 10CAL-1.2-0.5 after 8 cycles of tensile training at varying strains.

cyclic strain (%)	Tensile strength (MPa)	Elongation at break (%)	Toughness (MJ/m^3)	Enhancement rate (%)
Original	42.8 (±1.7)	1569 (±25)	270.5	—
600	59.4 (±3.6)	1150 (±94)	276.6	38.8
1000	64.5 (±2.8)	1230 (±107)	329.1	50.7
1200	43.4 (±1.2)	991 (±28)	185.0	1.4

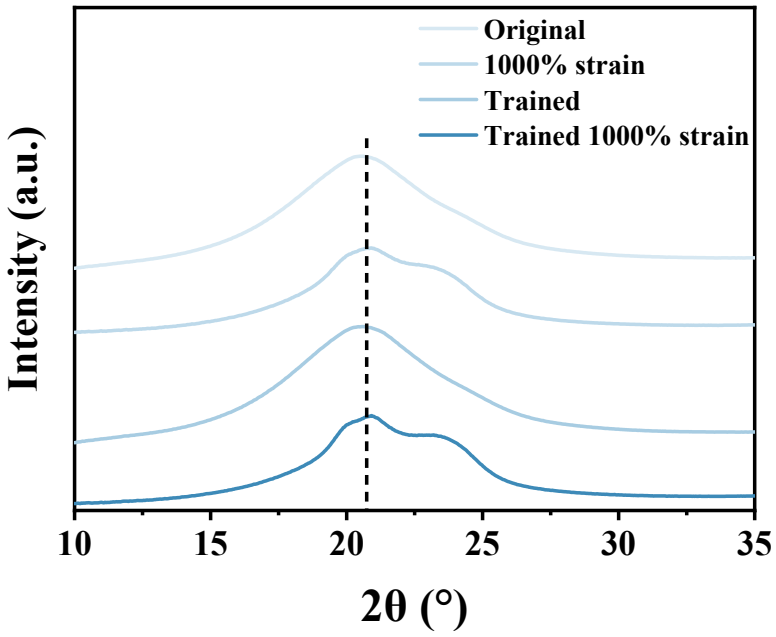

Figure S8. 1D WAXD profiles of 10CAL-1.2-0.5.

Table S7. Herman orientation factors of 10CAL-1.2-0.5 and 10CAL-1.2-0 under different states.

Sample	Original	1000% strain	Trained	Trained 1000% strain
10CAL-1.2-0.5	0.022	0.213	0.050	0.243
10CAL-1.2-0	0.022	0.195	0.034	0.222

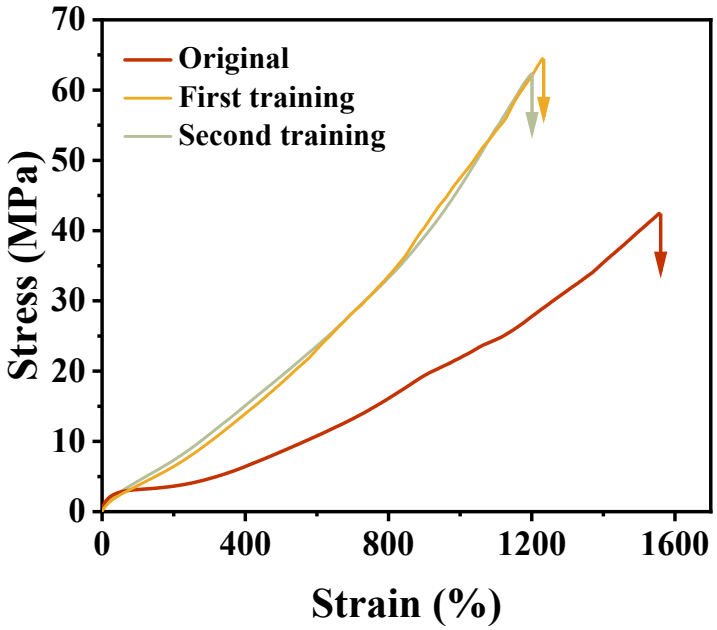

Figure S9. Stress-strain curves of 10CAL-1.2-0.5 after the first and second training.

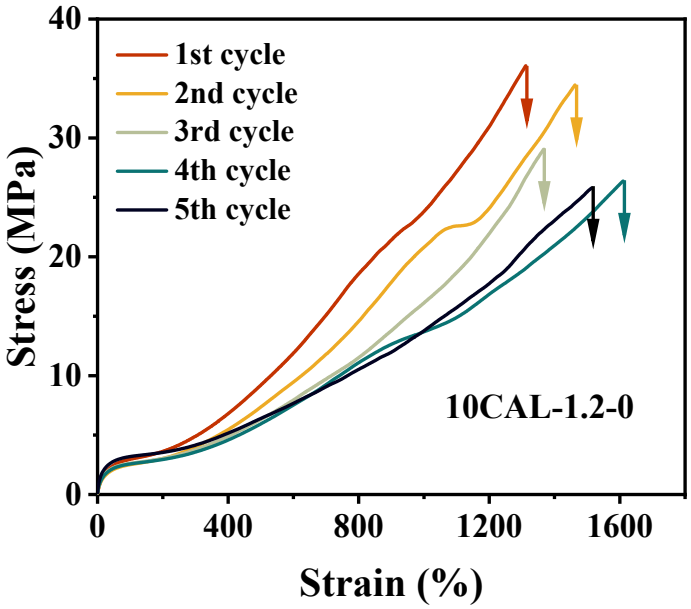

Figure S10. Stress-strain curves of 10CAL-1.2-0 before and after 5 hot pressing cycles.

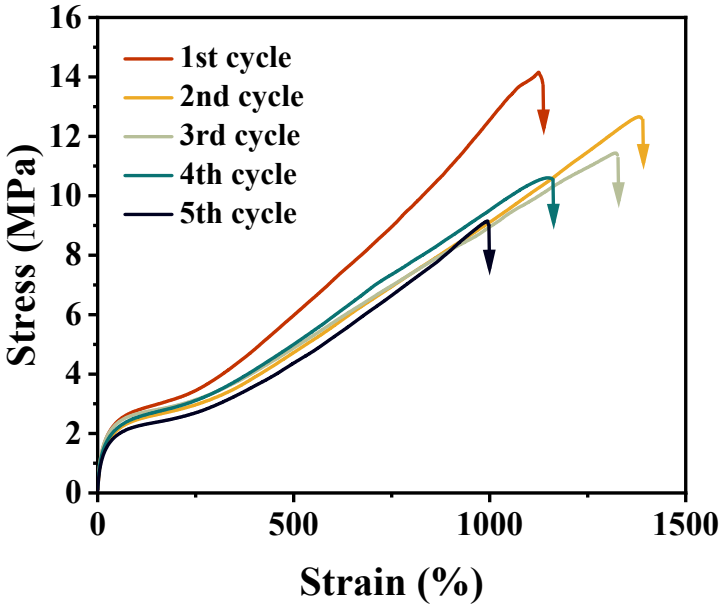

Figure S11. Stress-strain curves of 10AOH-1.2-1 before and after 5 hot pressing cycles.

Table S8. Reprocessing performance of Zn-LPUes.

Sample	Number of hot pressing	Tensile strength (MPa)	Retention rate of tensile strength (%)	Elongation at break (%)	Retention rate of elongation at break (%)	Toughness (MJ/m^3)	Retention rate of toughness (%)
10CAL-1.2-0	1st	37.9 (±3.6)	—	1408 (±76)	—	198.9	—
	2nd	34.5 (±1.4)	91.0	1464 (±101)	104.0	208.5	104.8
	3rd	29.0 (±2.3)	76.5	1368 (±95)	97.2	152.5	76.7
	4th	26.4(±2.7)	69.3	1532 (±147)	109.0	184.8	92.9
	5th	23.5 (±3.1)	62.0	1298 (±122)	92.2	169.5	85.2
10CAL-1.2-0.5	1st	42.8 (±1.7)	—	1569 (±25)	—	270.5	—
	2nd	41.7 (±2.5)	97.4	1488 (±144)	94.8	264.7	97.8
	3rd	37.6 (±2.2)	87.9	1546 (±88)	98.5	226.1	83.6
	4th	36.5 (±1.4)	85.3	1574 (±106)	100.3	232.7	86.0
	5th	34.5 (±2.3)	80.6	1583 (±36)	100.9	206.2	76.2
10AOH-1.2-1	1st	14.2 (±2.1)	—	1135 (±80)	—	107.2	—
	2nd	12.7 (±1.7)	89.4	1381 (±122)	121.7	92.4	86.2
	3rd	11.4 (±2.4)	80.3	1321 (±106)	116.4	84.5	78.8
	4th	10.6 (±1.5)	74.6	1147 (±97)	101.1	69.0	64.4
	5th	9.2 (±0.6)	64.8	1013 (±53)	89.3	47.4	44.2

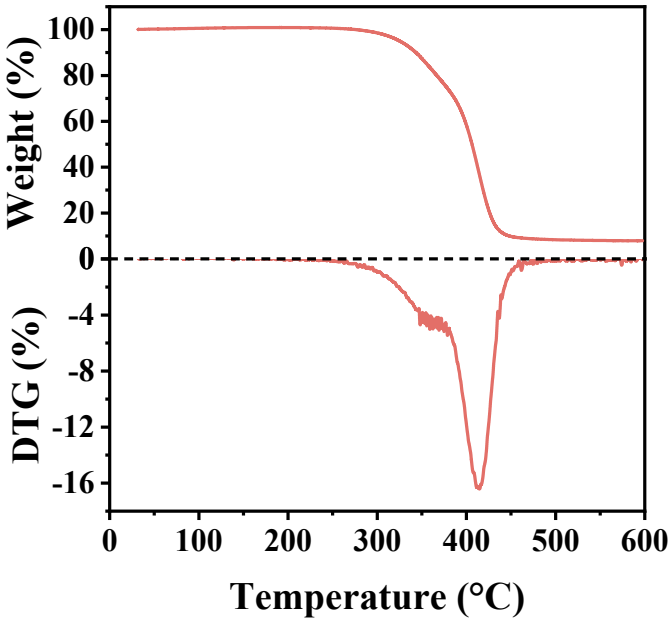

Figure S12. TG and DTG curves of 10CAL-1.2-0.5 after 5 hot pressing.

Table S9. Reprocessing performance of 10CAL-1.2-0.5.

Number of hot pressing	Tensile strength (MPa)	Retention rate of tensile strength (%)	Elongation at break (%)	Retention rate of elongation at break (%)	Toughness (MJ/m^3)	Retention rate of toughness (%)
1st	42.8 (±1.7)	—	1569 (±25)	—	270.5	—
2nd	41.7 (±2.5)	97.4	1488 (±144)	94.8	264.7	97.8
3rd	37.6 (±2.2)	87.9	1546 (±88)	98.5	226.1	83.6
4th	36.5 (±1.4)	85.3	1574 (±106)	100.3	232.7	86.0
5th	34.5 (±2.3)	80.6	1583 (±36)	100.9	206.2	76.2
6th	32.8 (±0.8)	76.6	1482 (±24)	94.5	186.1	68.8
7th	30.2 (±1.1)	70.6	1670 (±101)	106.4	243.0	89.8

8th	28.5 (±1.9)	66.6	1644 (±97)	104.8	216.3	80.0
9th	26.1 (±1.4)	61.0	1438 (±15)	91.7	156.0	57.7

Table S10. Comparison between 10CAL-1.2-0.5 and other reported petroleum-based and bio-based polyurethane elastomers: SF-LPU,[2] L1.0P9.0T0.2Zn,[3] PU-TREN-$Fe_{0.5}$,[4] PIDB-1,[5] $SPU_{0.5}$,[6] LVPU10,[7] PUA-HVPOH.[8]

Sample	Material type	Dynamic bond design	Tensile strength (MPa)	Tensile strength retention ratio (%)
10CAL-1.2-0.5	bio-based	phenol-carbamate bonds, metal-coordination bonds and hydrogen bonds	42.8	97.4
SF-LPU	bio-based	hydrogen bonds	6.4	95.2
L1.0P9.0T0.2Zn	bio-based	metal-coordination bonds and hydrogen bonds	31.4	92
PU-TREN-$Fe_{0.5}$	petroleum-based	metal-coordination bonds, imine bonds and hydrogen bonds	54.9	46
PIDB-1	petroleum-based	borate ester bonds and hydrogen bonds	24.3	88
$SPU_{0.5}$	petroleum-based	hydrogen bonds	38.2	70.2
LVPU10	bio-based	imine bonds and	26.2	91.6

		hydrogen bonds		
PUA-HVPOH	bio-based	oxime-urethane bonds and hydrogen bonds	42.3	54.3

Table S11. DMA data of Zn-LPUes.

Sample	υ_e (mol/m^3)	$T_{g\text{-}DMA}$ (°C)
10CAL-1.2-0	9646.2	-44.6
10CAL-1.2-0.5	13238.8	-49.2
10CAL-1.2-1	8140.2	-45.7

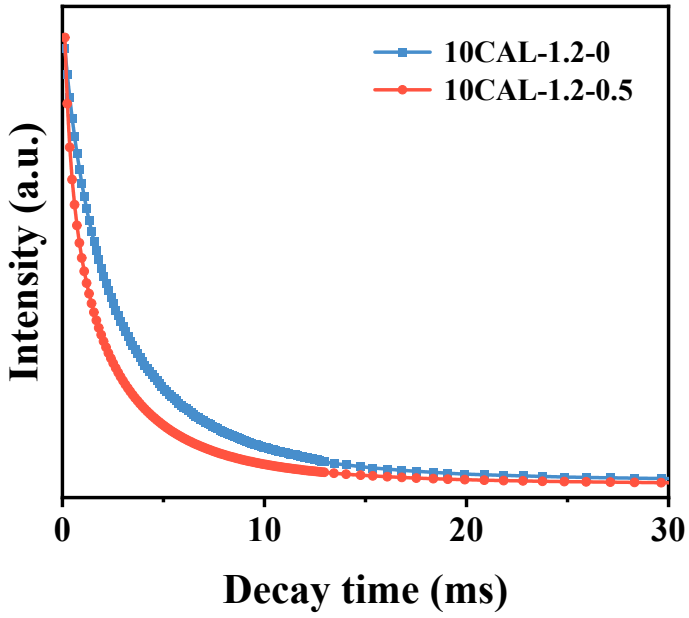

Figure S13. low-field NMR spectra of Zn-LPUes.

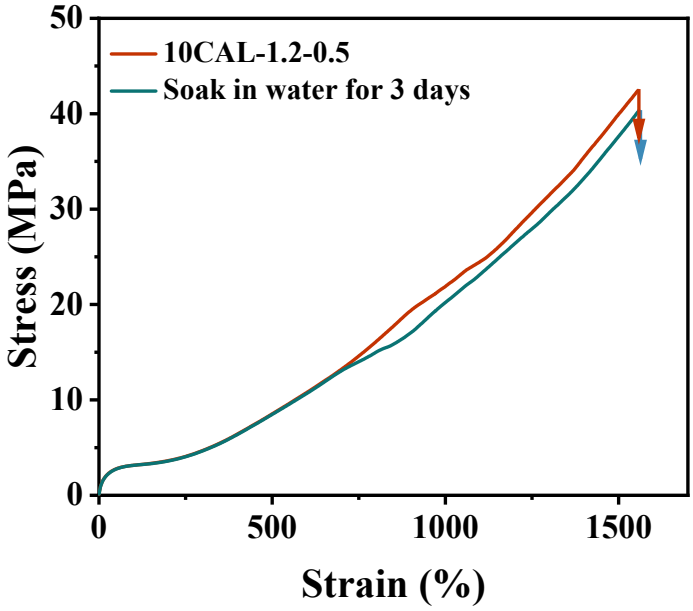

Figure S14. Stress-strain curves of 10CAL-1.2-0.5 before and after soaking in water for 3 days.

Table S12. Mechanical properties of 10CAL-1.2-0.5 before and after soaking in water for 3 days.

Method	Tensile strength (MPa)	Retention rate of tensile strength (%)	Elongation at break (%)	Retention rate of elongation at break (%)
Original	42.8	—	1569	—
Soak in water for 3 days	40.3 (±0.8)	94.2	1559 (±32)	99.4

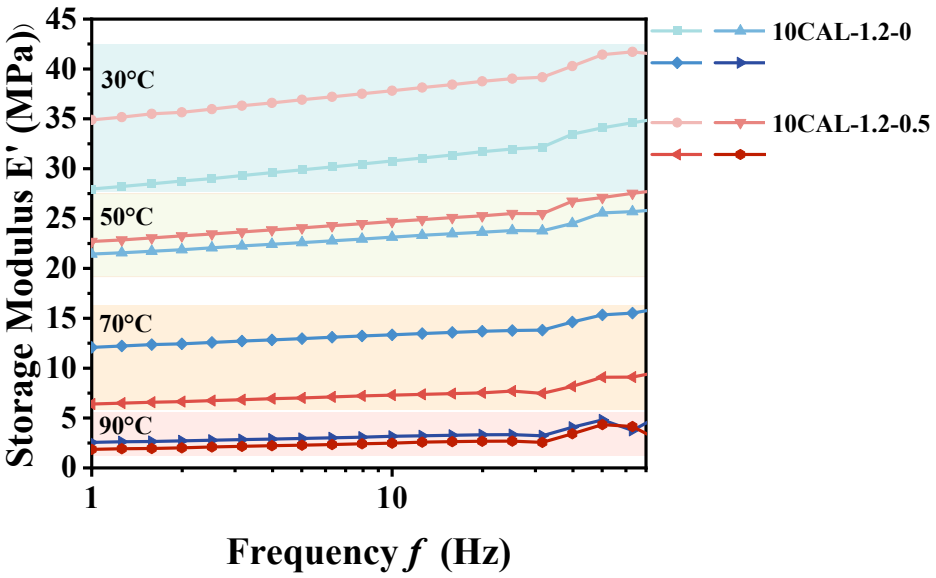

Figure S15. Dependences of storage modulus (E') on frequency for Zn-LPUes.

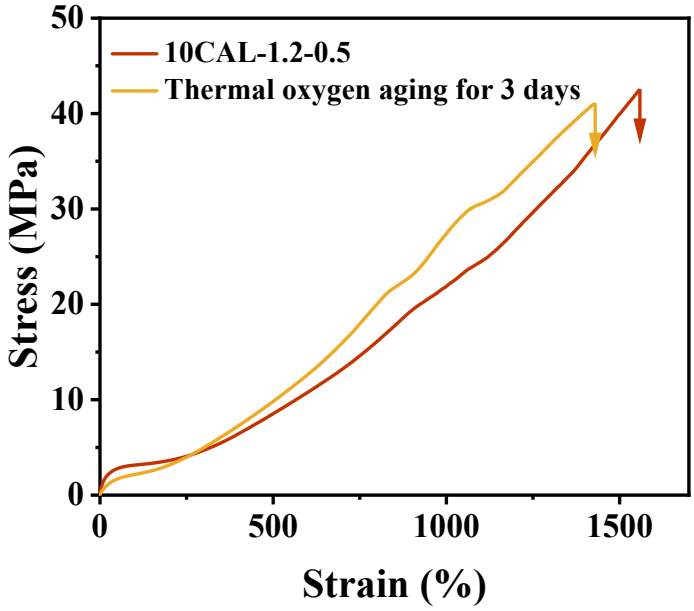

Figure S16. Stress-strain curves of 10CAL-1.2-0.5 before and after thermal oxygen aging for 3 days.

Table S13. Mechanical properties of 10CAL-1.2-0.5 before and after thermal oxygen aging for 3 days.

Method	Tensile strength (MPa)	Retention rate of tensile strength (%)	Elongation at break (%)	Retention rate of elongation at break (%)
Original	42.8	—	1569	—
Thermal oxygen aging for 3 days	41.0 (±1.3)	95.8	1425 (±89)	90.8

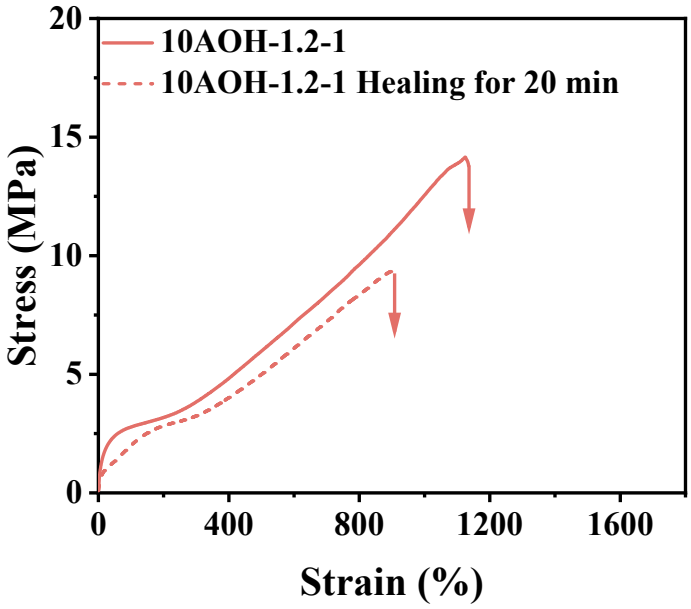

Figure S17. Stress-strain curves of 10AOH-1.2-1 before and after NIR-assisted self-healing at 0.5 W/cm^2 for 20 minutes.

Table S14. Mechanical properties of Zn-LPUes before and after healing at 0.5 W/cm^2.

Sample	Healing time (min)	Tensile strength (MPa)	Retention rate of tensile strength (%)	Elongation at break (%)	Retention rate of elongation at break (%)
10CAL-1.2-0	—	37.9 (±3.6)		1408 (±76)	
	20	29.5 (±1.6)	77.8	1098 (±68)	78.0
10CAL-1.2-0.5	—	42.8 (±1.7)	—	1569 (±25)	—
	20	32.0 (±2.3)	74.8	1465 (±92)	93.4
10AOH-1.2-1	—	14.2 (±2.1)	—	1135 (±80)	—
	20	9.3 (±0.8)	65.5	904 (±31)	79.6

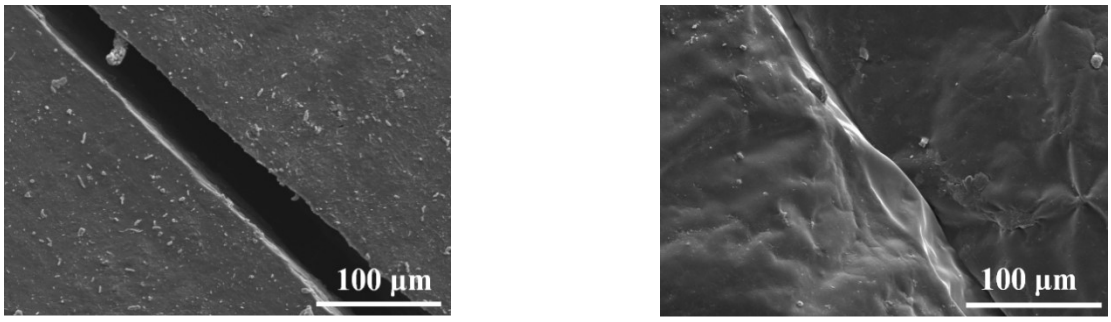

Figure S18. SEM images of 10CAL-1.2-0.5 before and after 20 minutes NIR-assisted healing at 0.5 W/cm^2 for 20 minutes.

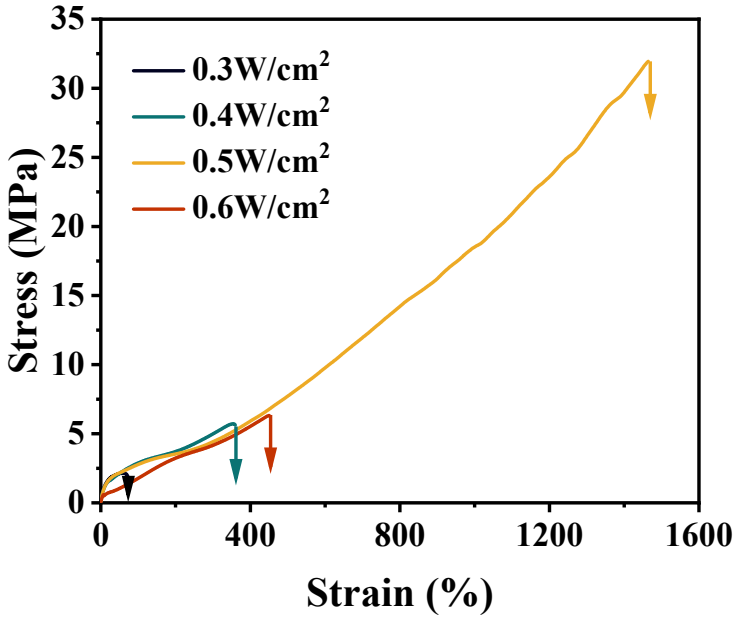

Figure S19. Stress-strain curves of 10CAL-1.2-0.5 before and after healing for 20 minutes under different NIR laser power densities.

Table S15. Mechanical properties of 10CAL-1.2-0.5 after healing for 20 minutes under different NIR laser power densities.

NIR laser power densities (W/cm^2)	maximum temperature rise ΔT_{max} (°C)	Tensile strength (MPa)	Retention rate of tensile strength (%)	Elongation at break (%)	Retention rate of elongation at break (%)
—	—	42.8 (±1.7)	—	1569 (±25)	—
0.3	45	2.2 (±1.9)	5.1	58 (±6)	3.7
0.4	105	5.7 (±3.7)	13.3	354 (±13)	22.6
0.5	180	32.0 (±2.3)	74.8	1465 (±92)	93.4
0.6	268	6.3 (±2.9)	14.7	450 (±58)	28.7

Table S16. Mechanical properties of 10CAL-1.2-0.5 after healing for different times under 0.5 W/cm^2.

Healing time (min)	Tensile strength (MPa)	Retention rate of tensile strength (%)	Elongation at break (%)	Retention rate of elongation at break (%)
—	42.8 (±1.7)	—	1569 (±25)	—
10	20.7 (±2.5)	48.4	1043 (±77)	66.5
20	32.0 (±2.3)	74.8	1465 (±92)	93.4
30	16.2 (±1.1)	37.9	862 (±18)	54.9

References

1. J. Peng, H. Wang, S. Chen, W. Liu and X. Qiu, *Macromolecules*, 2025, **58**, 836-854.
2. J. Huang, H. Wang, W. Liu, J. Huang, D. Yang, X. Qiu, L. Zhao, F. Hu and Y. Feng, *Int. J. Biol. Macromol.*, 2023, **225**, 1505-1516.
3. H. Wang, J. Huang, W. Liu, J. Huang, D. Yang, X. Qiu and J. Zhang, *Macromolecules*, 2022, **55**, 8629-8641.
4. X. Mou, Y. Guo, X. Lai, J. Ding, H. Li and X. Zeng, *Macromol. Rapid Commun.*, 2025, **29**, e00509.
5. T. Zhang, S. Huo, G. Ye, C. Wang, Q. Zhang and Z. Liu, *React. Funct. Polym.*, 2024, **205**, 106056.
6. Z. Li, D. Feng, D. Li, L. Zhou, C. Ge and X. Zhang, *Small*, 2025, **21**, 2504828.
7. Z. Huang, D. Han, G. Yi, W. Lin, X. Lin, Y. Sun and H. Wang, *Adv. Funct. Mater.*, 2025, **35**, 2507845.
8. H. Ding, L. Liu, C. Wang, N. Sun, L. Wu, B. Lin, K. Zhou, W. Zhang, X. Qian, C. Shi and B. Yu, *Chem. Eng. J.*, 2025, **514**, 163416.